A hybrid variational-perturbation calculation of the ro-vibrational spectrum of nitric acid

A. I. Pavlyuchko, S. N. Yurchenko, and Jonathan Tennyson

Citation: J. Chem. Phys. **142**, 094309 (2015); doi: 10.1063/1.4913741
View online: https://doi.org/10.1063/1.4913741
View Table of Contents: http://aip.scitation.org/toc/jcp/142/9
Published by the American Institute of Physics

A hybrid variational-perturbation calculation of the ro-vibrational spectrum of nitric acid

A. I. Pavlyuchko,[1,2,a)] S. N. Yurchenko,[1] and Jonathan Tennyson[1]
[1]*Department of Physics and Astronomy, University College London, London WC1E 6BT, United Kingdom*
[2]*Department of Physics, Moscow State University of Civil Engineering (MGSU), Moscow, Russia*

(Received 20 December 2014; accepted 17 February 2015; published online 5 March 2015)

Rotation-vibration spectra of the nitric acid molecule, HNO_3, are calculated for wavenumbers up to 7000 cm^{-1}. Calculations are performed using a Hamiltonian expressed in internal curvilinear vibrational coordinates employing a hybrid variational-perturbation method. An initial potential energy surface (PES) and dipole moment function (DMF) are calculated *ab initio* at the CCSD(T)/aug-cc-pVQZ level of theory. Parameters of the PES and DMF are varied to minimize differences between the calculated and experimental transition frequencies and intensities. The average, absolute deviation between calculated and experimental values is 0.2 cm^{-1} for frequencies in the fundamental bands and 0.4 cm^{-1} for those in the first overtone and lowest combination bands. For the intensities, the calculated and experimental values differ by 0.3% and 40% for the fundamentals and overtones, respectively. The optimized PES and DMF are used to calculate the room-temperature ro-vibrational spectrum. These calculation reproduce both the form of the absorption bands and fine details of the observed spectra, including the rotational structure of the vibrational bands and the numerous hot absorption band. Many of these hot bands are found to be missing from the compilation in HITRAN. A room temperature line list comprising 2×10^9 lines is computed. © *2015 AIP Publishing LLC.* [http://dx.doi.org/10.1063/1.4913741]

I. INTRODUCTION

Nitric acid (HNO_3), in spite of its low concentration, makes a significant contribution to the infrared (IR) spectrum of the earth's atmosphere, since it has a number of strong absorption bands lying in the water transparency window.[1–6] Yet, its spectrum remains poorly characterized with, for example, no transition wavenumbers above 2000 cm^{-1} included in the HITRAN database,[7] despite the fact that several fundamental bands lie at higher wavenumbers. This issue is not due to any lack of attempts to measure the IR spectrum of HNO_3,[8–51] but rather to do with the difficulty of interpreting its spectrum and making line assignments. Experimental line intensities have also been the subject of number of studies.[19,39,44,46,52–56]

The study of the HNO_3 spectrum over a range of temperatures is a difficult experimental and theoretical problem. Experimental study of the HNO_3 IR spectrum is challenging because in the gas phase, it is a mixture containing significant numbers of dimers and complexes, as well as the products of its dissociation (NO_2, H_2O, O_2). Therefore, experimental HNO_3 spectra are usually reduced spectra in which spectra due to dimers, complexes, and dissociation products have been subtracted. In addition, HNO_3 is a chemically aggressive species, which greatly complicates the experimental study of its spectrum at higher temperatures.

From the theoretical perspective, study of the ro-vibrational infrared spectrum of the HNO_3 is difficult because of the relatively large number of the vibrational degrees of freedom, $N_c = 9$, and the large anharmonicity of its vibrations. There are only limited attempts to solve the vibrational and ro-vibrational problems using full-dimensionality.[47,57–60] Benderskii and Vetoshkin[57] used a perturbative approach to study the tunneling dynamics of internal rotation. Lauvergnat and Nauts[58] also concentrated on these levels in both reduced and full dimensionality. Konen *et al.*[47] used second-order vibrational perturbation theory (VPT2) to help interpreting their experimental findings. More recently, Avila and Carrington[59,60] have performed full-dimensional variational calculations with a particular focus on how to make such studies efficient. None of these studies considered transition intensities and amongst various *ab initio* studies using more approximate treatments,[61–66] only Lee and Rice[61] appear to have considered (harmonic) intensities.

Recently, we[67] developed a hybrid variational-perturbational calculation scheme for computing IR spectra of polyatomic species. HNO_3 was one of the species used to test this methodology. Here, we present semi-empirical calculations of the infrared spectrum of HNO_3 performed using this method. The calculations provide a comprehensive room temperature line list covering the range 0-7000 cm^{-1}.

II. HAMILTONIAN

Our vibration-rotation Hamiltonian written in curvilinear internal coordinates and an Eckart embedding has the form[68]

$$\hat{H}_{vr} = \hat{H}_v - \frac{\hbar^2}{2} \sum_{a,b} \frac{\partial}{\partial \xi_a} \mu_{ab}(\underline{q}) \frac{\partial}{\partial \xi_b}, \quad \xi_a, \xi_b = \alpha, \beta, \gamma, \qquad (1)$$

a)pavlyuchko@rambler.ru

TABLE I. Elements of the $\underline{G}(\underline{q})$ matrix for two classes of nonlinear bending coordinate φ, where m_1, m_2, and m_3 are the atomic masses, r_1 is the length of the bond between atoms 1 and 3, and r_2 the length of the bond between atoms 2 and 3.

	$\varphi = -\Delta \arccos\left(\frac{\vec{r}_1\vec{r}_2}{r_1 r_2}\right)$	$\varphi = -\Delta\left(\frac{\vec{r}_1\vec{r}_2}{r_1 r_2}\right)$
$g_{r_1 r_1}$	$\left(\frac{1}{m_1}+\frac{1}{m_3}\right)$	$\left(\frac{1}{m_1}+\frac{1}{m_3}\right)$
$g_{r_2 r_2}$	$\left(\frac{1}{m_2}+\frac{1}{m_3}\right)$	$\left(\frac{1}{m_2}+\frac{1}{m_3}\right)$
$g_{r_1 r_2} = g_{r_2 r_1}$	$\frac{\cos(\varphi)}{m_3}$	$\frac{\varphi}{m_3}$
$g_{r_1\varphi} = g_{\varphi r_1}$	$\frac{\sin(\varphi)}{r_2 m_3}$	$\frac{(1-\varphi^2)}{r_2 m_3}$
$g_{r_2\varphi} = g_{\varphi r_2}$	$\frac{\sin(\varphi)}{r_1 m_3}$	$\frac{(1-\varphi^2)}{r_1 m_3}$
$g_{\varphi\varphi}$	$\frac{1}{r_1^2}\frac{m_1+m_3}{m_1 m_3} + \frac{1}{r_2^2}\frac{m_2+m_3}{m_2 m_3} + \frac{2[(\cos(\varphi))^2-\cos(\varphi)]}{(\sin(\varphi))^2 r_1 r_2 m_3}$	$\frac{(1-\varphi^2)}{r_1^2}\frac{m_1+m_3}{m_1 m_3} + \frac{(1-\varphi^2)}{r_2^2}\frac{m_2+m_3}{m_2 m_3} + \frac{2(\varphi^2-\varphi)}{r_1 r_2 m_3}$

where $\underline{\xi}$ are the rotational coordinates and $\hat{H}_v$ is the vibrational part of the Hamiltonian

$$\hat{H}_v = \hat{T}_v + V(\underline{q}), \tag{2}$$

$$\hat{T}_v = -\frac{\hbar^2}{2}\sum_{i,j} t^{\frac{1}{4}}\frac{\partial}{\partial q_i} g_{ij}(\underline{q}) t^{-\frac{1}{2}}\frac{\partial}{\partial q_j} t^{\frac{1}{4}}. \tag{3}$$

Here, q_i are internal, vibrational curvilinear coordinates given by changes in the bond lengths, valence bond angles, and dihedral angles from the corresponding equilibrium values; α, β, γ are the Euler angles between the axes of the equilibrium moment of inertia tensor and external Cartesian coordinate axes; $\mu_{ab}(\underline{q})$ are elements of the inverse of the moment of inertia tensor, $\underline{I}(\underline{q})$; $\hat{T}_v$ is the vibrational kinetic energy operator and $g_{ij}(\underline{q})$ are elements of the kinetic energy coefficients matrix $\underline{G}(\underline{q})$ and $t = \det[\underline{G}]$. Finally, $V(\underline{q})$ is the molecular potential energy.

After transformation, the vibrational kinetic operator can be written as

$$\hat{T}_v = -\frac{\hbar^2}{2}\sum_{i,j}\frac{\partial}{\partial q_i} g_{ij}(\underline{q})\frac{\partial}{\partial q_j} + \beta(\underline{q}), \tag{4}$$

where

$$\begin{aligned}\beta(\underline{q}) = -\frac{\hbar^2}{2}\sum_{i,j}\Bigg\{&\frac{\partial g_{ij}(\underline{q})}{\partial q_i}\sum_{k,l}\zeta_{kl}(\underline{q})\frac{\partial g_{kl}(\underline{q})}{\partial q_j} \\ &+ \frac{1}{4}g_{ij}(\underline{q})\Bigg[\sum_{k,l}\zeta_{kl}(\underline{q})\frac{\partial^2 g_{kl}(\underline{q})}{\partial q_i \partial q_j} \\ &- \sum_{k,l,m,n}\zeta_{kl}(\underline{q})\zeta_{mn}(\underline{q})\Bigg(\frac{\partial g_{lm}(\underline{q})}{\partial q_i}\frac{\partial g_{kn}(\underline{q})}{\partial q_j} \\ &+ \frac{\partial g_{kl}(\underline{q})}{\partial q_i}\frac{\partial g_{mn}(\underline{q})}{\partial q_j}\Bigg)\Bigg]\Bigg\}\end{aligned} \tag{5}$$

is the pseudo-potential or Watson term;[69] $\zeta_{ij}(\underline{q})$ are elements of $\underline{G}(\underline{q})^{-1}$.

We have performed calculations[68,70] which suggest that pseudo-potential Eq. (5) makes only a small contribution to the vibrational energy levels of polyatomic molecules such as HNO_3. For the water molecule, this contribution is less than 1.3, 1.0, and 1.9 cm^{-1} for the fundamental energy levels ν_1, ν_2, and ν_3, respectively. With the growth in the size of the molecule and increase in its total mass, the contribution of the pseudo-potential to the vibrational energy levels decreases significantly.[68] Therefore, to simplify and speed-up the calculations, we neglect the contribution of the pseudo-potential. Some of this contribution will be incorporated in our final, empirical potential energy surface (PES).

Elements of the $\underline{G}(\underline{q})$ matrix are, in general, a complicated function of the vibrational coordinates.[68] As an example, Table I gives elements of $\underline{G}(\underline{q})$ for the stretching and bending (inter-bond angle) modes. The latter in the case of HNO_3 are the angles ∠ N-O-N and N-O-H. The elements of $\underline{G}(\underline{q})$ are presented for two cases: for the bending coordinates given in the form of $\varphi = -\Delta \arccos\left(\frac{\vec{r}_1\vec{r}_2}{r_1 r_2}\right)$ and in the form of its cosine, $\varphi = -\Delta\left(\frac{\vec{r}_1\vec{r}_2}{r_1 r_2}\right)$. In total for HNO_3 there are 55 elements of $\underline{G}(\underline{q})$.

As can be seen from Table I, expressing the bending coordinates as a change in the angle leads to a simplified expression for the matrix elements of $\underline{G}(\underline{q})$ because their dependence on φ is a linear or quadratic. However, in general, $\underline{G}(\underline{q})$ is a complicated function of the internal coordinates. General expressions of its elements are given elsewhere.[68] In general terms, if both coordinates represent changes in bond lengths then

$$g_{ij}(\underline{q}) = g^0_{ij}(\underline{\varphi}), \tag{6}$$

if one coordinate represents a change in the bond length and the second is an angular coordinate then

$$g_{ij}(\underline{q}) = \sum_k \frac{1}{r_k} g^k_{ij}(\underline{\varphi}), \tag{7}$$

and if both represent angular coordinates, it becomes

$$g_{ij}(\underline{q}) = \sum_{k,l}\frac{1}{r_k r_l} g^{kl}_{ij}(\underline{\varphi}). \tag{8}$$

In these expressions, r_k is the bond length of the kth bond and $\underline{\varphi}$ represents the angular coordinates.

$\underline{G}(\underline{q})$ is computed using a second-order Taylor expansion in the angular coordinates

$$g_{ij}(\underline{q}) = g^0_{ij}(0) + \sum_m \left(\frac{\partial g^0_{ij}(\underline{\varphi})}{\partial \varphi_m}\right)_0 \varphi_m + \frac{1}{2}\sum_{m,n}\left(\frac{\partial^2 g^0_{ij}(\underline{\varphi})}{\partial\varphi_m\partial\varphi_n}\right)_0 \varphi_m\varphi_n, \quad (9)$$

for the case where i and j both represent bonds,

$$g_{ij}(\underline{q}) = \sum_k \frac{1}{r_k}\left[g^k_{ij}(0) + \sum_m \left(\frac{\partial g^k_{ij}(\underline{\varphi})}{\partial \varphi_m}\right)_0 \varphi_m + \frac{1}{2}\sum_{m,n}\left(\frac{\partial^2 g^k_{ij}(\underline{\varphi})}{\partial\varphi_m\partial\varphi_n}\right)_0 \varphi_m\varphi_n\right], \quad (10)$$

for the case of one bond and one angle,

$$g_{ij}(\underline{q}) = \sum_{k,l} \frac{1}{r_k r_l}\left[g^{kl}_{ij}(0) + \sum_m \left(\frac{\partial g^{kl}_{ij}(\underline{\varphi})}{\partial \varphi_m}\right)_0 \varphi_m + \frac{1}{2}\sum_{m,n}\left(\frac{\partial^2 g^{kl}_{ij}(\underline{\varphi})}{\partial\varphi_m\partial\varphi_n}\right)_0 \varphi_m\varphi_n\right] \quad (11)$$

for two angles. It is beneficial to choose an internal coordinate in $\underline{\varphi}$ as cosine differences $q_i = \cos\varphi_i - \cos\varphi^e_i$, where $\cos\varphi^e_i$ is the instantaneous equilibrium angle for bond angles. As can be seen from Table I, these expansions in terms of $\underline{\varphi}$ are exact as $g^0_{ij}(\underline{\varphi})$, $g^k_{ij}(\underline{\varphi})$, and $g^{kl}_{ij}(\underline{\varphi})$ are quadratic functions of the angular coordinates. In this expansion, a sine difference $q_i = \sin\varphi_i - \sin\varphi^e_i$ is the obvious choice for an internal coordinate describing a dihedral mode.

To simplify the calculation of the vibrational Hamiltonian matrix elements in block 2 (see below), which correspond to the perturbative contribution for the matrix elements from the main block 1 (see below), the vibrational kinetic energy coefficients are expanded in the polynomial form and truncated at second order

$$g_{ij}(\underline{q}) = g_{ij}(0) + \sum_m \left(\frac{\partial g_{ij}(\underline{q})}{\partial q_m}\right)_0 q_m + \frac{1}{2}\sum_{m,n}\left(\frac{\partial^2 g_{ij}(\underline{q})}{\partial q_m\partial q_n}\right)_0 q_m q_n. \quad (12)$$

This form is convenient because it allows faster, by an order-of-magnitude or more, computation of the coefficients without significant loss of accuracy.

The potential energy function used by us is a fourth-order polynomial

$$V(\underline{q}) = \frac{1}{2}\sum_{i,j} D_{ij}x_i x_j + \frac{1}{6}\sum_{i,j,k} D_{ijk}x_i x_j x_k + \frac{1}{24}\sum_{i,j,k,l} D_{ijkl}x_i x_j x_k x_l, \quad (13)$$

where Morse coordinates, $x_i = (1 - \exp^{-\alpha_i \Delta r_i})$, are used to represent changes of all bonds for HNO_3 molecule and $x_i = q_i$ for angular coordinates.

III. METHOD

For ease of use and better convergence of the basis functions, the χ_i are generally chosen to form a complete orthonormal set. In variational calculations of vibrational energy levels, the Hamiltonian matrix elements are computed using the product form

$$\chi_{kn} = \prod_i \phi_{k_i}(r_i)\prod_s \psi_{n_s}(Q_s) \quad (14)$$

of the basis functions, which are eigenfunctions of the Morse or harmonic oscillators. Morse oscillator functions, $\phi_{k_i}(r_i)$, are used for the stretching coordinates, r_i, for which the potential is given using a Morse coordinate. Harmonic basis functions, $\psi_{n_s}(Q_s)$, are used for the other coordinates, which are represented using curvilinear normal coordinates

$$Q_s = \sum_i L^q_{is} q_i \quad (15)$$

expressed as a linear sum over the internal coordinates, q_i, for which the potential function is defined as a Taylor series. The coordinates Q_s are those which diagonalize the harmonic part of the Hamiltonian given in the internal coordinates q_i. With these definitions, all multi-dimensional integrals required to calculate the Hamiltonian matrix elements are separated into products of one-dimensional integrals between either Morse functions or harmonic oscillators. All these integrals have a simple analytic form which results in high-speed computation of the Hamiltonian matrix elements.

The vibrational Hamiltonian matrix constructed in this way is then diagonalized to give the vibrational energy levels E^{vib}_λ and the corresponding wave functions ϕ^{vib}_λ.

Our implementation relies on the particular structure of the Hamiltonian matrix ordered by increasing polyad (total vibrational excitation) number, N_V,

$$N_V = \sum_{m=1}^{N_c} a_m v_m, \quad (16)$$

where a_m is some weighting which is often roughly proportional to the inverse of the frequency.[71] For simplicity, in this work, we use $a_m = 1$ for all m. This gives the size of the basis set, $M^{\max}_B$ in terms of the maximum polyad number, $N^{\max}_V$,

$$M^{\max}_B = \frac{(N^{\max}_V + N_c)!}{N^{\max}_V! N_c!} = \prod_{i=1}^{N_c}(N^{\max}_V + i)/i. \quad (17)$$

Calculating all $N_V \le N^{\text{target}}_V$ vibrational term values for HNO_3 with an accuracy better than 0.3 cm^{-1} requires basis functions with $N^{\max}_V \ge N^{\text{target}}_V + 9$. This means that the Hamiltonian matrix must include all the basis functions for which the difference in v_m is larger than 9. Thus, an accurate calculation of the fourth overtones and combination frequencies ($N^{\text{target}}_V = 5$) demands a variational basis for HNO_3 ($N_c = 9$) which includes $M^{\max}_B = 817\,190$ basis functions.

We use a hybrid variational-perturbation method for calculating ro-vibrational energy levels of a polyatomic molecules.[67] It combines the advantages of both variational calculations and perturbation theory. The vibrational problem is solved by diagonalizing a Hamiltonian matrix, which is partitioned into two sub-blocks, as shown in Fig. 1. The first,

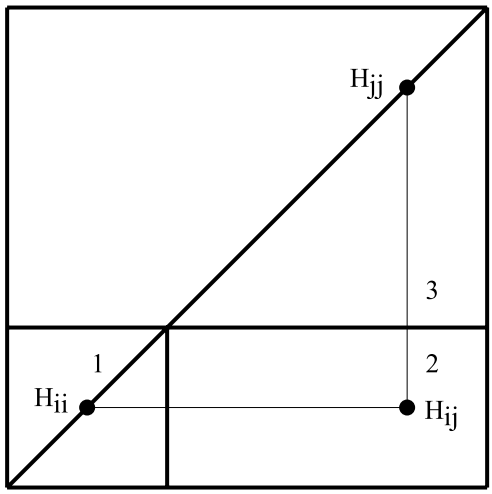

FIG. 1. Block structure of the vibrational Hamiltonian matrix. Region 1: matrix elements with the largest contributions to the target energy levels ($N_V \le N_v^{\text{target}}+4$); region 2 contains elements with small contributions to these states. The contribution from elements in region 3 is disregarded.

smaller sub-block includes matrix elements with the largest contribution to the energy levels targeted in the calculations ($N_V \le N_v^{\text{target}} + 4$). The second, larger sub-block comprises those basis states which have little effect on these energy levels. Numerical perturbation theory, implemented as a Jacobi rotation, is used to compute the contributions from the matrix elements of the second sub-block. Only the first sub-block needs to be stored in memory and diagonalized. The size of block 1, $M_B^{(1)}$, is given by Eq. (17) using $N_V^{(1)}$ as the number of the largest polyad included in block 1.

In the first step of our approach, all the matrix elements from blocks 1 are computed along with the diagonal matrix elements of block 3. The second step involves computing the off-diagonal elements of block 2 and accounting for their effect on the matrix elements of the block 1 using one Jacobi rotation.[72,73] Considering a contribution from the off-diagonal element H_{ij} in block 2, which couples the diagonal elements H_{ii} in block 1 and H_{jj} in block 3, the diagonal element in block 1 is perturbatively adjusted using the Jacobi formula

$$\tilde{H}_{ii} = H_{ii} - \sum_{j\in\text{block2}} \Delta E_{ij}, \tag{18}$$

where

$$\Delta E_{ij} = \frac{\text{sign}(\sigma_{ij})H_{ij}}{|\sigma_{ij}| + \sqrt{1+\sigma_{ij}^2}} \tag{19}$$

and

$$\sigma_{ij} = \frac{(H_{jj} - H_{ii})}{2H_{ij}}. \tag{20}$$

For ro-vibrational energy levels, it is necessary to calculate elements of the complex Hermitian Hamiltonian matrix

$$H^{JJ'}_{\lambda k m,\lambda' k' m'} = \langle \chi^J_{\lambda k m} | \hat{H}_{vr} | \chi^{J'}_{\lambda' k' m'} \rangle, \tag{21}$$

using the basis functions

$$\chi^J_{\lambda k m} = \Phi^{vib}_{\lambda} \phi^J_{km}, \quad \phi^J_{km} = \left(\frac{2J+1}{8\pi^2}\right)^{1/2} D^{J\,*}_{km}, \tag{22}$$

where D^J_{km} is a (complex) Wigner function. In this case,

$$H^J_{\lambda k,\lambda' k'} = E^{vib}_{\lambda}\delta_{\lambda\lambda'}\delta_{kk'} - \frac{\hbar^2}{2}\sum_{a,b}\bar{\mu}^{\lambda\lambda'}_{ab}\langle\phi^J_{km}|\frac{\partial^2}{\partial\xi_a\partial\xi_b}|\phi^J_{k'm}\rangle. \tag{23}$$

The vibrationally averaged moment of inertia, $\bar{\mu}^{\lambda\lambda'}_{ab}$, is expanded to second-order as a Taylor series,

$$\begin{aligned}\bar{\mu}^{\lambda\lambda'}_{ab} &= \langle\Phi^{vib}_{\lambda}|\mu_{ab}(\underline{q})|\Phi^{vib}_{\lambda'}\rangle \\ &= \mu_{ab}(0)\delta_{\lambda\lambda'} + \sum_m \left(\frac{\partial\mu_{ab}(\underline{q})}{\partial q_m}\right)_0 \langle\Phi^{vib}_{\lambda}|q_m|\Phi^{vib}_{\lambda'}\rangle \\ &\quad + \frac{1}{2}\sum_{m,n}\left(\frac{\partial^2\mu_{ab}(\underline{q})}{\partial q_m\partial q_n}\right)_0 \langle\Phi^{vib}_{\lambda}|q_m q_n|\Phi^{vib}_{\lambda'}\rangle\end{aligned} \tag{24}$$

and all the integrals reduce to products of one-dimensional integrals over either Morse or harmonic oscillators.

The off-diagonal elements of the vibration-rotation Hamiltonian matrix,

$$H^J_{\lambda k,\lambda' k'} = -\frac{\hbar^2}{2}\sum_{a,b}\bar{\mu}^{\lambda\lambda'}_{ab}\langle\phi^J_{km}|\frac{\partial^2}{\partial\xi_a\partial\xi_b}|\phi^J_{k'm'}\rangle, \tag{25}$$

differ significantly in magnitude, depending on whether they are diagonal in the vibrations, $\lambda = \lambda'$, or couple different vibrational states, $\lambda \ne \lambda'$.

When calculating the vibrational-rotational energy levels, the off-diagonal elements $H^J_{\lambda k,\lambda' k'}$ corresponding to different vibrational states $\lambda \ne \lambda'$ give a much smaller contribution (change in the diagonal elements in the block that will be diagonalized) to the calculated energy levels than the off-diagonal elements $H^J_{\lambda k,\lambda k'}$ within the vibrational state in question. These changes are given approximately by

$$\Delta E_{\lambda\lambda'} = \frac{\left(H^J_{\lambda k,\lambda' k'}\right)^2}{H^J_{\lambda' k',\lambda' k'} - H^J_{\lambda k,\lambda k}}, \tag{26}$$

$$\Delta E_{\lambda\lambda} = \frac{\left(H^J_{\lambda k,\lambda k'}\right)^2}{H^J_{\lambda k',\lambda k'} - H^J_{\lambda k,\lambda k}}. \tag{27}$$

However,

$$|H^J_{\lambda' k',\lambda' k'} - H^J_{\lambda k,\lambda k}| \gg |H^J_{\lambda k',\lambda k'} - H^J_{\lambda k,\lambda k}| \tag{28}$$

since $(H^J_{\lambda k',\lambda k'} - H^J_{\lambda k,\lambda k})$ involves only a change in the rotational energy level, while $(H^J_{\lambda' k',\lambda' k'} - H^J_{\lambda k,\lambda k})$ involves also a change in the vibrational energy level. For semi-rigid molecules with small values of the vibrational quantum numbers, the following condition usually holds

$$|H^J_{\lambda k,\lambda k'}| > |H^J_{\lambda k,\lambda' k'}|, \quad \lambda \ne \lambda', \tag{29}$$

which results from the slight change in the effective geometry of the molecule upon vibrational excitation. This feature of the vibrational-rotational Hamiltonian matrix is common for large molecules and underpins the ro-vibrational version of our hybrid approach.[67] Again, we use second-order perturbation theory, as defined by a Jacobi rotation, to transform the $H^J_{\lambda k,\lambda' k'}$ matrix to a series of much smaller rotational sub-matrices corresponding to different vibrational states λ, $\tilde{H}^J_{\lambda k,\lambda k'}$. The dimension of each rotational sub-block is $(2J+1)$ only and

we consider M_B^{target} sub-matrices that correspond to M_B^{target} vibrational states.

As above, we employ a single Jacobi rotation which we apply to the ro-vibrational Hamiltonian. The best agreement with the variational solution is achieved when both the diagonal and off-diagonal elements are updated[67] as given by

$$\tilde{H}^J_{\lambda k,\lambda k} = H^J_{\lambda k,\lambda k} + \sum_{\lambda' \in M_B^{\text{vib}},\lambda' \neq \lambda} \sum_{k'} t_{\lambda k,\lambda' k'} \eta_{\lambda k,\lambda' k'} \tag{30}$$

for the diagonal elements and

$$\begin{aligned}\tilde{H}^J_{\lambda k,\lambda k''} = \frac{1}{2} \sum_{\lambda' \in M_B^{\text{vib}},\lambda' \neq \lambda} \sum_{k'} \Big[& c_{\lambda k,\lambda' k'} H^J_{\lambda k,\lambda k''} \\ & + c_{\lambda k'',\lambda' k'} H^{*J}_{\lambda k,\lambda k''} + s_{\lambda k,\lambda' k'} H^J_{\lambda' k',\lambda k''} \\ & + s_{\lambda' k',\lambda k''} H^J_{\lambda k,\lambda' k'} \Big],\end{aligned} \tag{31}$$

for the off-diagonal elements. Equation (31) is a symmetrized version of the standard formula for the single Jacobi rotation with respect to the indices λk and $\lambda k''$. In the above expressions,

$$\begin{aligned} c_{\lambda k,\lambda' k'} &= \frac{1}{\sqrt{1 + t^2_{\lambda k,\lambda' k'}}}, \\ s_{\lambda k,\lambda' k'} &= \frac{c_{\lambda k,\lambda' k'} t_{\lambda k,\lambda' k'}}{\eta_{\lambda k,\lambda' k'}} H^J_{\lambda k,\lambda' k'}, \\ t_{\lambda k,\lambda' k'} &= \text{sign}(\vartheta_{\lambda k,\lambda' k'}) / (|\vartheta_{\lambda k,\lambda' k'}| + \sqrt{1 + \vartheta^2_{\lambda k,\lambda' k'}}), \\ \eta_{\lambda k,\lambda' k'} &= \text{sign}\left[\text{Re}(H^J_{\lambda k,\lambda' k'})\right] |H^J_{\lambda k,\lambda' k'}|, \\ \vartheta_{\lambda k,\lambda' k'} &= \frac{H^J_{\lambda k,\lambda k} - H^J_{\lambda' k',\lambda' k'}}{2\eta_{\lambda k,\lambda' k'}}, \end{aligned}$$

where $\underline{H}^J$ and $\underline{\tilde{H}}^J$ are the initial (unperturbed) matrix and perturbed matrix, respectively; λ runs from 1 to M_B^{target}, and $k = -J, \ldots, +J$.

The resulting block-diagonal form is then diagonalized for each λ sub-matrix separately. Thus, our algorithm replaces the diagonalization of a huge $[M_B^{\text{vib}} \times (2J+1)]$-dimensional ro-vibrational matrix with a number of diagonalizations of much smaller dimensional-$[(2J+1)]$ matrices.

IV. POTENTIAL ENERGY AND DIPOLE MOMENT FUNCTIONS

An important factor in solving the anharmonic vibrational problem is the choice of internal curvilinear vibrational coordinates, q_i. This choice determines how close the truncated polynomial potential function of Eq. (13) is to the real PES of the molecule, as well as the specific form of the kinetic energy coefficients matrix, $\underline{G}(q)$, see Eqs. (9)–(11).

The structure of the HNO_3 molecule and the atom numbering we use are shown in Fig. 2. For HNO_3, we employ the following vibrational coordinates.

- Four coordinates represent changes in the length of valence bonds between atoms

$$\Delta r_i = \left\{\Delta r_{\text{NO}_a}, \Delta r_{\text{NO}_b}, \Delta r_{\text{NO}_c}, \Delta r_{\text{O}_c\text{H}}\right\},$$

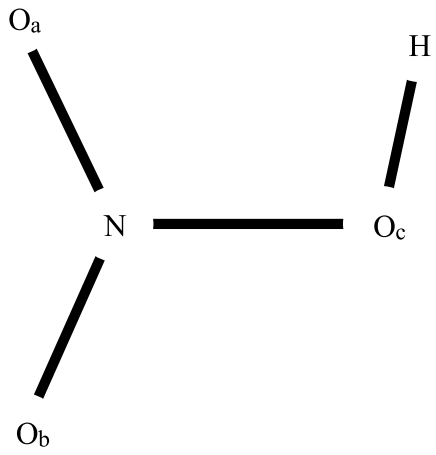

FIG. 2. Structure of the HNO_3 molecule.

where

$$r_i = \left\{r_{\text{NO}_a}, r_{\text{NO}_b}, r_{\text{NO}_c}, r_{\text{O}_c\text{H}}\right\}$$

are lengths of the bond vectors

$$\vec{r}_i = \left\{\vec{r}_{\text{NO}_a}, \vec{r}_{\text{NO}_b}, \vec{r}_{\text{NO}_c}, \vec{r}_{\text{O}_c\text{H}}\right\}$$

with the vectors pointing from the first to the second atom.

- Four coordinates represent changes in the cosines of angles between the valence bonds

$$\begin{aligned}\varphi_m = \Bigg\{ & -\Delta\left(\frac{\vec{r}_{\text{NO}_a}\vec{r}_{\text{NO}_b}}{r_{\text{NO}_a} r_{\text{NO}_b}}\right), -\Delta\left(\frac{\vec{r}_{\text{NO}_a}\vec{r}_{\text{NO}_c}}{r_{\text{NO}_a} r_{\text{NO}_c}}\right), \\ & -\Delta\left(\frac{\vec{r}_{\text{NO}_b}\vec{r}_{\text{NO}_c}}{r_{\text{NO}_b} r_{\text{NO}_c}}\right), -\Delta\left(\frac{\vec{r}_{\text{NO}_c}\vec{r}_{\text{O}_c\text{H}}}{r_{\text{NO}_c} r_{\text{O}_c\text{H}}}\right)\Bigg\}.\end{aligned}$$

This choice contains one dependent or redundant angle; this dependence is removed upon the introduction of Q_s coordinates, see Eq. (15).

- A coordinate corresponding to the change in the sine of the angle between the orientation of bond NO_c from the plane formed by bonds NO_a and NO_b,

$$\varphi_f = \Delta\left[\frac{\vec{r}_{\text{NO}_c}(\vec{r}_{\text{NO}_a} \times \vec{r}_{\text{NO}_b})}{r_{\text{NO}_c} r_{\text{NO}_a} r_{\text{NO}_b}}\right].$$

- A coordinate corresponding to the change in the sine of the angle between the plane formed by bonds NO_a, NO_b, and the plane formed by bonds NO_c and O_cH while rotating them relative to each other around NO_c bond

$$\varphi_\rho = \Delta\left\{\frac{\vec{\rho}\left[(\vec{r}_{\text{NO}_a} \times \vec{r}_{\text{NO}_b}) \times (\vec{r}_{\text{NO}_c} \times \vec{r}_{\text{O}_c\text{H}})\right]}{r_{\text{NO}_a} r_{\text{NO}_b} r_{\text{NO}_c} r_{\text{O}_c\text{H}}}\right\},$$

where $\vec{\rho}$ is a unit vector perpendicular to the equilibrium plane of the molecule.

This physically motivated choice of internal curvilinear vibrational coordinates ensures that quartic expansion of the potential, Eq. (13), stays close to the real PES in the region around the minimum. For example, HNO_3 has a low frequency mode, ν_9, corresponding to rotation of the O_cH bond around the NO_c bond which is approximately represented by the coordinate φ_ρ. This vibrational mode is characterized

TABLE II. Experimental (Expt.)[28] and calculated (Calc.) vibrational term values for excitation of the ν_9 mode using *ab initio* potential parameters; the result of Lauvergnat and Nauts[58] are given for comparison.

Transition	Frequency (cm^{-1})		
	Expt.	Calc.[58]	Our calc.
ν_9	458.2	458.0	456.7
$2\nu_9$	896.3	886.6	894.1
$3\nu_9$	1289.0	1293.1	1284.2
$4\nu_9$	1664.7	1671.9	1656.7

by very large anharmonicity, as it has large amplitude and a strongly anharmonic potential function. Quantum-chemical calculations carried out by Lauvergnat and Nauts[58] show that this rotation corresponds to the potential curve which is close to a sine wave. Our quantum-chemical calculations show that in the expansion of the PES as a function of coordinate φ_ρ in Eq. (13) gives a nonzero quadratic term for coordinate φ_ρ but zero cubic and quartic terms. This is because writing the potential function in the form $V(\varphi_\rho) = \frac{1}{2} D_{\varphi_\rho\varphi_\rho} \varphi_\rho^2$ is equivalent to defining it as a sine wave in the angle of rotation of the O_cH bond. Thus, choosing the vibrational coordinates in the form of change of sine of the angle for this mode provides a compact definition of the strongly anharmonic sinusoidal potential function as a single term in the expansion Eq. (13). As a result, we obtain good agreement between the experimental and calculated vibrational terms values for $n\nu_9$ using our *ab initio* potential parameter, see Table II. This in turn means that the calculated spectrum reproduces the absorption intensities for the hot bands starting from the ν_9, $2\nu_9$, $3\nu_9$ states which are shifted from the main absorption bands and which are characteristic of HNO_3, see Figure 5 and discussion below.

We use a simplified method for the initial calculation of parameters for the PES and dipole moment function (DMF). This simplification is justified because our neglect of the pseudo-potential as well as other small contributions such as adiabatic effects.[74] This means that we cannot calculate energy levels *ab initio* with the accuracy needed to compute a final line list. Therefore, it is necessary to improve the PES and DMF semi-empirically by solving the inverse spectral problem.

First, we compute a force constant expansion for the PES using a fourth-order Taylor series

$$V(\underline{q}) = \frac{1}{2}\sum_{i,j} f_{ij}^0 q_i q_j + \frac{1}{6}\sum_{i,j,k} f_{ijk}^0 q_i q_j q_k + \frac{1}{24}\sum_{i,j,k,l} f_{ijkl}^0 q_i q_j q_k q_l \quad (32)$$

in internal curvilinear coordinates q_i. Initial values for the quadratic force constants f_{ij}^0 were calculated using the central finite difference relations

$$f_{ii}^0 = \frac{E^+ + E^- - 2E^0}{\delta q_i^2}, \quad f_{ij}^0 = \frac{E^{++} + E^{--} - E^{+-} - E^{-+}}{4\delta q_i \delta q_j}, \quad (33)$$

where E^0 is the molecular energy of the equilibrium configuration and $E^\pm$ is the energy of the geometry in which the vibrational coordinate q_i is increased/decreased by δq_i. E^{++}, E^{--}, E^{+-}, E^{-+} are energies for geometries in which the vibrational coordinates q_i and q_j are increased and/or decreased by multiples of δq_i and δq_j. Energies and the equilibrium geometry of HNO_3 were calculated *ab initio* at the CCSD(T)/aug-cc-pVQZ level of theory using MOLPRO.[75] Similarly, the initial values of cubic f_{ijk}^0 and quartic f_{ijkl}^0 force constants were calculated using the finite difference relations

$$f_{ijk}^0 = \frac{f_{ij}^+ + f_{ij}^- - 2f_{ij}^0}{\delta q_k^2}, \quad f_{ijkl}^0 = \frac{f_{ij}^{++} + f_{ij}^{--} - f_{ij}^{+-} - f_{ij}^{-+}}{4\delta q_k \delta q_l}, \quad (34)$$

where f_{ij}^0 are the Hessian (quadratic force constants) at the equilibrium geometry, $f_{ij}^\pm$ is the Hessian corresponding to an increase/decrease in the vibrational coordinates q_i by δq_i. The Hessians f_{ij}^{++}, f_{ij}^{--}, f_{ij}^{+-}, f_{ij}^{-+} are computed at geometries obtained by increasing and decreasing vibrational coordinates q_i and q_j by multiples of δq_i and δq_j. These Hessians were calculated *ab initio* at the MP2/aug-cc-pVQZ level of theory using Gaussian.[76] These calculations were based on the MP2/aug-cc-pVQZ equilibrium geometry.

The second step of the calculation uses the initial force constants f_{ij}^0, f_{ijk}^0, f_{ijkl}^0 to construct the constants D_{ij}, D_{ijk}, D_{ijkl} which are used to represent the PES, see Eq. (13). This requires taking into account the relation between the f, D, and α constants for the Morse oscillator, for example, $f_{ii}^0 = D_{ii}\alpha_i^2$.

In the third stage of the calculation, the PES parameters are refined using the empirical values of the energy levels. Solution of the inverse spectral problem is facilitated by the analytic evaluation of the first derivatives of the energy levels, E_i, with respect to PES parameters D_j using the Hellmann-Feynman theorem,

$$\frac{\partial E_i}{\partial D_j} = \langle\psi_i|\frac{\partial \hat{H}_v}{\partial D_j}|\psi_i\rangle = \langle\psi_i|\frac{\partial V(q)}{\partial D_j}|\psi_i\rangle, \quad (35)$$

where ψ_i is the wave function of energy level E_i.

Our solution of the inverse spectral problem is based on the method of regularization due to Tikhonov.[77,78] This method minimizes the functional

$$\Phi = \sum_i \left(E_i^c - E_i^e\right)^2 W_i + \sum_j \left[\alpha_j \left(\frac{D_j - D_j^0}{\Delta D_j^{\max}}\right)^2 + \beta_j \left(\frac{D_j - D_j^0}{\Delta D_j^{\max}}\right)^{10}\right], \quad (36)$$

where E_i^c, E_i^e, and W_i are the calculated and experimental values of the energy level and its weight, D_j and D_j^0 are the current and initial values of the parameters, and $\Delta D_j^{\max}$ is the maximum possible deviation of parameter value from its initial value. In this formula, α_j and β_j are regularization parameters that allow one to control progress in solving the inverse problem. The terms containing D_j in this functional allows one to constrain the refined parameters to their initial (*ab initio*) values. The method of regularization ensures that there is always a valid solution, even when the number of experimental energies is less than the number of variable parameters. This is similar to the method where the shape of the potential functions are controlled by constraining directly to the *ab initio* energies (see, for example Ref. 79.

The dipole moment of HNO_3 is represented as a second-order polynomial

$$\vec{D}(\underline{q}) = \vec{D}^0 + \sum_i \vec{d}_i q_i + \frac{1}{2}\sum_{i,j} \vec{d}_{ij} q_i q_j, \tag{37}$$

where $\vec{D}^0$ is the equilibrium value of the dipole moment, $\vec{d}_i$ and $\vec{d}_{ij}$ equal, respectively, the first and second derivatives of the dipole moment with respect to the curvilinear coordinates q_i and q_j. Initial values of $\vec{d}_i$ and $\vec{d}_{ij}$ were calculated using the finite difference relations

$$\vec{d}_i = \frac{\vec{D}^+ + \vec{D}^- - 2\vec{D}^0}{\delta q_i^2}, \quad \vec{d}_{ij} = \frac{\vec{D}^{++} + \vec{D}^{--} - \vec{D}^{+-} - \vec{D}^{-+}}{4\delta q_i \delta q_j}, \tag{38}$$

where $\vec{D}^{\pm}$ is the dipole moment corresponding to an increase/decrease in the vibrational coordinates q_i by δq_i. Dipole moments $\vec{D}^{++}$, $\vec{D}^{--}$, $\vec{D}^{+-}$, $\vec{D}^{-+}$ correspond to the geometries obtained by increasing or decreasing vibrational coordinates q_i and q_j by multiples of δq_i and δq_j. Dipole moments were calculated *ab initio* at the CCSD(T)/aug-cc-pVQZ level of theory using MOLPRO from the change in energy of the molecule in an external electric field, which is considered the better of the methods for computing *ab initio* dipoles.[80]

Calculation of initial values of the PES and DMF parameters and all subsequent calculations were made using program ANGMOL.[68] ANGMOL automatically produces the necessary inputs for MOLPRO and Gaussian, runs these programs and extracts the required data (energy, Hessian, and dipole moment) from their listings. These calculations take into account the relationship between our internal curvilinear coordinates, q_i, and the Cartesian coordinates of the atoms.[68]

The calculated initial values of the force constants and the dipole moment of the molecule depend on the increment, δq_i, used to evaluate the derivatives. For small values of δq_i, these derivatives are distorted by the finite numerical precision inherent in Gaussian and MOLPRO, while for large increments, the PES and DMF may not be quadratic. We find that optimal increments, δq_i, are 0.01 Å for bonds and 0.01 for changes in cosines and sines of the angular coordinates. These increments were used in all calculations of the initial PES and DMF coefficients.

Ro-vibrational calculations showed that the CCSD(T)/aug-cc-pVQZ equilibrium geometry does not accurately describe the rotational energy levels. Therefore, we used a modified geometry in which all bond lengths were reduced by 0.1%. Table III gives our calculated and modified equilibrium geometry.

Finally, we note that the program ANGMOL is freely available on upon request to the first author.

TABLE III. Equilibrium bond lengths (Å) and angles (°) in the molecule HNO_3 which is planar.

Parameter	*Ab initio*	Modified
r_{NO_a}	1.210 32	1.209 11
r_{NO_b}	1.195 31	1.194 12
r_{NO_c}	1.399 60	1.398 20
r_{O_cH}	0.969 85	0.968 88
α_{NO_a,NO_b}	130.271 3	130.271 3
α_{NO_a,NO_c}	115.719 9	115.719 9
α_{NO_b,NO_c}	114.008 8	114.008 8
$\alpha_{NO_c,OH}$	102.204 0	102.204 0

V. CALCULATED VIBRATIONAL TERM VALUES

First, the vibrational energy levels were calculated using the Hamiltonian described in Sec. II and our hybrid variational-perturbation method,[67] as implemented in ANGMOL.[68]

An important feature of the HNO_3 IR spectrum[28,43,81] in the 0-7000 cm^{-1} range is that absorption is dominated by the fundamental (ν_i), first overtones ($2\nu_i$), and first combination ($\nu_i + \nu_j$) bands. The presence of low-frequency vibrations with high anharmonicity also leads to observation of hot band transitions, such as $4\nu_i$-$3\nu_i$ and $4\nu_i$-$2\nu_i$, even at room temperature. The strongest hot-band transitions correspond to those involving the low-frequency ν_9 mode. In addition, the spectrum is further complicated by strong Fermi resonances, for example, between ν_5 and $2\nu_9$.

We aim to make accurate calculations (better than 1 cm^{-1}) for vibrational states with the quantum numbers up to $N_V^{\text{target}} = 5$ which corresponds to $M_B^{\text{target}} = 2002$ vibrational states. This means we must include in the fully diagonalized block 1 all states with $N_V^{(1)} \le 9$ which gives $M_B^{(1)} = 48\,620$. The total size of the basis corresponds to $N_V^{\max} = 14$ and $N_B^{\max} = 817\,190$ functions. Computing the elements of block 2, whose size is $M_B^{(1)} \times M_B^{\max} = 48\,620 \times 817\,190$, and including them as a perturbation takes 3 h on an 8-core desktop computer. This is cheap compared to the subsequent diagonalization of the 48 620 dimensional matrix.

Table IV shows the calculated and experimental vibrational term values for the HNO_3 molecule. These calculations were carried out with our initial, *ab initio*, PES. As can be seen, this PES gives a generally satisfactory description of the experimental vibrational term values. The average deviation between the calculated and experimental fundamental energy levels is 3 cm^{-1}. For the first overtone and combination levels, it is 6 cm^{-1}. The calculation describes the strong Fermi resonance between ν_5 and $2\nu_9$ well.

However, this accuracy is not sufficient to generate a good line list. Therefore, we have refined the PES parameters using the method of regularization. The parameters α_i, which define the half-width of the Morse functions for the stretching coordinates, were fixed in the fits to their *ab initio* values. The inverse problem was solved in two steps. First, 39 quadratic parameters of the potential function, D_{ij} of Eq. (13), were refined using the 11 equally weighted vibrational term values: the fundamentals plus $2\nu_9$ and $\nu_6 + \nu_9$. The results of this fit are given as calculation II in Table IV. The average deviation between calculated and experimental fundamental levels energy is now less than 0.2 cm^{-1} and is about 3 cm^{-1} for the first overtone and first combination bands.

In the second stage, all potential parameters D_{ij}, D_{ijk}, and D_{ijkl} are varied: a total of 584 parameters were refined using the 46 experimental term values, given in Table IV. Following the method of regularization, we use 584 additional constraints for these parameters to their initial *ab initio* D_{ijk} and D_{ijkl}

TABLE IV. Experimental and calculated vibrational term values, in cm^{-1}, for HNO_3. Calculation I is based on the *ab initio* parameters, while calculations II and III are the two sets of the refined potential parameters, see text. The references give the source of the experimental data used, but see text for a discussion of the actual values given.

State		I	II	III	Expt.	Source
A''	ν_9	456.7	458.2	458.2	458.2	28
A'	ν_8	577.0	580.3	580.4	580.3	38
A'	ν_7	647.3	646.7	647.0	646.5	38
A''	ν_6	770.1	763.2	763.3	763.1	81
A'	ν_5	876.7	879.1	878.8	879.1	81
A'	$2\nu_9$	894.1	896.4	896.2	896.3	81
A''	$\nu_8+\nu_9$	1025.0	1029.9	1038.0	1038.0	81
A''	$\nu_7+\nu_9$	1096.0	1097.0	1100.3	1100.8	81
A'	$\nu_6+\nu_9$	1210.2	1205.4	1205.2	1205.6	81
A''	$3\nu_9$	1284.2	1288.8	1289.6	1289.0	28
A'	ν_4	1303.0	1302.9	1303.2	1303.1	81
A'	ν_3	1329.6	1326.2	1326.3	1325.7	81
A''	$\nu_5+\nu_9$	1337.5	1340.5	1343.7	1343.6	28
A'	$\nu_7+\nu_5$	1507.9	1509.9	1516.0	1515.9	81
A'	$2\nu_6$	1539.2	1525.4	1525.4	1525.6	81
A'	$\nu_7+2\nu_9$	1526.1	1528.2	1533.7	1533.2	81
A'	$4\nu_9$	1656.7	1662.8	1661.3	1664.7	28
A'	ν_2	1716.4	1709.5	1709.4	1709.6	81
A'	$2\nu_5$	1747.1	1751.3	1757.0	1757.0	81
A'	$\nu_5+2\nu_9$	1769.9	1773.9	1780.4	1780.3	81
A''	$\nu_3+\nu_9$	1790.2	1788.0	1789.2	1789.7	81
A'	$\nu_3+\nu_8$	1900.6	1900.4	1905.8	1906.0	81
A'	$\nu_4+\nu_7$	1941.4	1940.8	1949.2	1949.6	81
A'	$\nu_3+\nu_7$	1968.4	1964.3	1974.7	1975.2	81
A''	$\nu_4+\nu_6$	2066.5	2059.7	2061.4	2061.4	81
A''	$\nu_3+\nu_6$	2102.4	2091.5	2091.9	2092.0	81
A''	$\nu_2+\nu_9$	2174.5	2169.7	2165.2	2164.8	81
A'	$\nu_2+\nu_5$	2537.5	2531.0	2530.8	2530.6	43
A'	$2\nu_4$	2584.2	2582.1	2580.5	2580.9	43
A'	$\nu_2+2\nu_9$	2595.2	2593.2	2596.2	2596.5	43
A'	$2\nu_3$	2651.0	2644.0	2643.8	2644.4	43
A'	$\nu_2+\nu_4$	3003.2	2998.2	2998.4	2998.5	43
A'	$\nu_2+\nu_3$	3033.3	3022.6	3021.8	3022.1	43
A'	$2\nu_2$	3411.2	3396.7	3404.2	3404.4	43
A'	ν_1	3553.3	3551.6	3551.6	3551.9	81
A''	$\nu_1+\nu_9$	4007.3	4007.3	4006.6	4007.0	43
A'	$\nu_1+\nu_8$	4125.5	4127.3	4127.4	4127.5	43
A'	$\nu_1+\nu_7$	4199.4	4196.3	4196.8	4197.0	43
A'	$2\nu_2+2\nu_9$	4319.1	4314.0	4315.0	4314.5	43
A'	$\nu_1+\nu_5$	4427.6	4428.2	4427.4	4427.6	43
A'	$\nu_1+2\nu_9$	4445.5	4446.0	4445.5	4445.8	43
A'	$2\nu_2+\nu_3$	4757.6	4751.5	4751.9	4750.0	43
A''	$\nu_1+3\nu_9$	4831.0	4833.4	4833.9	4832.8	43
A'	$\nu_1+\nu_4$	4870.7	4866.8	4865.5	4866.3	43
A'	$\nu_1+\nu_2$	5256.6	5248.2	5254.5	5252.4	43
A'	$2\nu_1$	6941.5	6935.1	6938.8	6940.0	43

values and to the values of D_{ij} obtained at the previous stage. This makes the inverse problem fully determined despite the small amount of experimental data. States with up to 3 quanta of excitation had weight 1.0, while 4 quanta states, whose energies are more uncertain, had a weight of 0.1. The results of this fit are shown as calculation III in Table IV. The average deviation between calculated and experimental fundamental levels energy remains 0.2 cm^{-1}, but for the first overtone and first combination bands, it is reduced to 0.4 cm^{-1}. This potential function was subsequently used to calculate the ro-vibrational energy levels and the line list.

We note that the "experimental" values of the vibrational term values given in Table IV do not match those given by Perrin *et al.*[28] or Feierabend *et al.*[43] This is because in these laboratory studies, the corresponding vibrational term values were estimated as band centers either as maxima of the Q-branches or minima between the P- and R-branches, and thus do not precisely correspond to the $J = 0$ energy of the

vibrationally excited state, because they also affected by the rotational structure. Therefore, Table IV gives our revised values: vibrational term values were determined as the energy, which, after their substitution in a full ro-vibrational calculation, gives coincidence between the computed and experimental rotational structure of the absorption band in question. These values should represent the best available estimate for the HNO_3 vibrational term values. Our estimated accuracy for the "experimental" vibrational term values given in Table IV is better than 0.1 cm^{-1}. The typical difference between our values and those given previously[28,43] is about 1 cm^{-1}, which corresponds to the half-width of a typical Q-branch. Finally, some experimental values given in Table IV do not come from high resolution spectra; these were identified by us from the observed absorption cross sections provided by PNNL.[81]

VI. CALCULATED RO-VIBRATIONAL SPECTRUM

We present the rotation-vibration spectrum in the range 0–7000 cm^{-1}, which includes all first overtones and first combination bands. To include all hot absorption bands present at room temperature, it was necessary to include all vibrational states lying below 9000 cm^{-1}.

There are about 20 000 vibrational states below 9000 cm^{-1}. Therefore, the calculation of ro-vibrational energy levels for all of these vibrational states and the calculation of intensities of allowed transitions between all the ro-vibrational levels is lengthy, even when using our hybrid method. Initially, this calculation took about 6 months on an 8-core desktop computer. However, as described below, this time can be reduced by two orders-of-magnitude by computing only those ro-vibrational energy levels and transition intensities which are actually needed. For concreteness, in what follows, we consider the explicit example of the calculation of a room temperature spectrum.

First, experimental, room-temperature spectra do not show any significant transitions to vibrational states with the polyad number $N_V > 4$, due to the very low intensity of such bands. Therefore, we only need to obtain results for the vibrational states with the polyad number $N_V^{\text{target}} \leq 4$. This reduces the number of vibrational states for which ro-vibrational energy levels are required to $M_B^{\text{target}} = 1715$. All other ro-vibrational states are only used to perturb the target ro-vibrational energy levels.

Second, not all of the 20 000 vibrational states below 9000 cm^{-1} actually significantly contribute the target ro-vibra-

TABLE V. Experimental and calculated intensities by region for HNO_3: experimental data are taken from PNNL,[81] HITRAN,[7] and Feierabend *et al.*[43] Calculation A used an *ab initio* DMF and calculation B a fitted DMF. The dominant bands for each frequency window are also given.

		Intensity (km/mol)				
Band	Frequency (cm^{-1})	Reference 7	Reference 81	Reference 43	Calc. A	Calc. B
Rotation	0-100	6.7			7.2	6.7
Hot	100-350				0.15	0.14
ν_9	350-520	77.7			107.3	77.7
ν_8	520-610	5.7			6.4	5.6
ν_7	610-700	5.6			13.2	5.6
ν_6	700-830	7.4			6.9	7.4
$\nu_5, 2\nu_9$	830-950	124.5	110.9		151.4	110.9
$\nu_8+\nu_9, \nu_7+\nu_9$	950-1140				0.53	0.82
$\nu_6+\nu_9$	1140-1240	5.7	7.9		8.7	7.9
$\nu_4, \nu_3, 3\nu_9, \nu_5+\nu_9$	1240-1380	229.3	221.6		300.4	220.8
$\nu_7+\nu_5, 2\nu_6, \nu_7+2\nu_9$	1380-1600		6.5		4.7	6.1
$\nu_2, 4\nu_9, 2\nu_5, \nu_5+2\nu_9, \nu_3+\nu_9$	1600-1825	263.5	251.8		354.0	251.4
$\nu_3+\nu_8, \nu_4+\nu_7, \nu_3+\nu_7$	1825-2040		1.5		3.4	1.8
$\nu_3+\nu_5, \nu_2+\nu_9$	2170-2240		0.37	0.44	0.67	0.38
$\nu_2+\nu_5, 2\nu_4, \nu_2+2\nu_9, 2\nu_3$	2460-2710		6.2	8.2	8.4	6.1
$\nu_2+\nu_4, \nu_2+\nu_3$	2920-3055		6.6	8.2	3.6	6.4
$2\nu_2$	3360-3440		1.3	1.6	0.51	1.3
ν_1	3490-3610		54.9	54.9	76.9	54.9
$3\nu_4, \nu_3+2\nu_4$	3828-3893		0.08	0.11	0.33	0.34
$\nu_1+\nu_9$	3950-4050		0.98	1.1	1.9	1.0
$\nu_1+\nu_8$	4075-4160		0.19	0.27	0.53	0.35
$2\nu_2+2\nu_9$	4230-4355		0.12	0.22	0.61	0.55
$\nu_1+\nu_5, \nu_1+2\nu_9$	4385-4490		0.13	0.16	0.20	0.18
$2\nu_2+\nu_3, 2\nu_2+\nu_4$	4630-4710		0.06	0.27	0.62	0.48
$2\nu_2+\nu_3$	4710-4780		0.13	0.11	0.67	0.24
$\nu_1+\nu_4, \nu_1+\nu_3, \nu_1+3\nu_9$	4790-4905		0.89	1.0	1.7	1.1
$3\nu_2$	5040-5115		0.06	0.05	0.59	0.50
$\nu_1+\nu_2$	5210-5290		0.33	0.33	0.52	0.40
$\nu_1+2\nu_4$	6080-6195		0.12	0.05	0.85	0.65
$2\nu_1, \nu_1+2\nu_2$	6865-7005			2.1	3.0	2.1

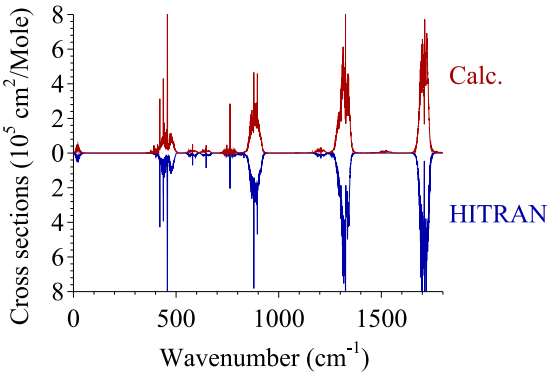

FIG. 3. Calculated (red curve) and HITRAN (blue curve) 296 K HNO_3 spectra in the 0-1800 cm^{-1} region.

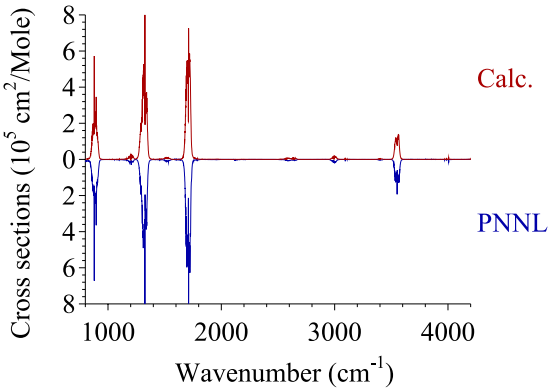

FIG. 4. Calculated (red curve) and experimental PNNL (blue curve) 298 K cross sections in the 800-4200 cm^{-1} region.

tional energy levels. This is because a large difference between the quantum numbers v_i^λ and $v_i^{\lambda'}$ from vibrational states λ and λ′ leads to vanishingly small values of the corresponding matrix elements $\bar{\mu}_{ab}^{\lambda\lambda'}$, Eq. (24), and $H^J_{\lambda k,\lambda' k'}$, Eq. (23). For example, for purely harmonic basis functions, the matrix elements $\bar{\mu}_{ab}^{\lambda\lambda'}$ and $H^J_{\lambda k,\lambda' k'}$ are exactly zero for $\sum_i |v_i^\lambda - v_i^{\lambda'}| > 2$. Using a mixed Morse-harmonic basis, we obtain $\bar{\mu}_{ab}^{\lambda\lambda'} \approx 0$ and $H^J_{\lambda k,\lambda' k'} \approx 0$ for $\sum_i |v_i^\lambda - v_i^{\lambda'}| > 3$. Therefore, only the contribution from the vibrational states with polyad numbers $N_V^{\text{vib}} \le 7$ needs to be evaluated as perturbation to the target ro-vibrational energy levels from the M_B^{vib} vibrational states. In this case, M_B^{vib} = 9477, which is only about half the vibrational states below 9000 cm^{-1}. Besides, when summing the perturbation effect for a given ro-vibrational energy levels, we can skip all pairs with $\sum_i |v_i^\lambda - v_i^{\lambda'}| > 3$. Therefore, the sums in Eqs. (30) and (31) for each value of λ will run over less than a tenth of all the levels included in M_B^{vib}.

Third, when considering a transition between different ro-vibrational states, it is useful to make a preliminary assessment of its intensity. If the estimated value is below some threshold, the intensity calculation can be skipped. Such intensities can be neglected either because of the small intrinsic value of the transition dipole or because of the low population of the initial ro-vibrational energy level caused by the Boltzmann factor. As, in large line lists, computation of the transition intensities dominates the computer time,[82] this significantly reduces the overall computer time.

When these three factors are taken into account, the time for computing the ro-vibrational spectrum in the 0–7000 cm^{-1} region is reduced from 6 months to 2 days on an 8-core desktop computer. This is quick enough even to allow us to refine our *ab initio* DMF by fitting to experimental line intensities, thus improving agreement between observed and computed spectra.

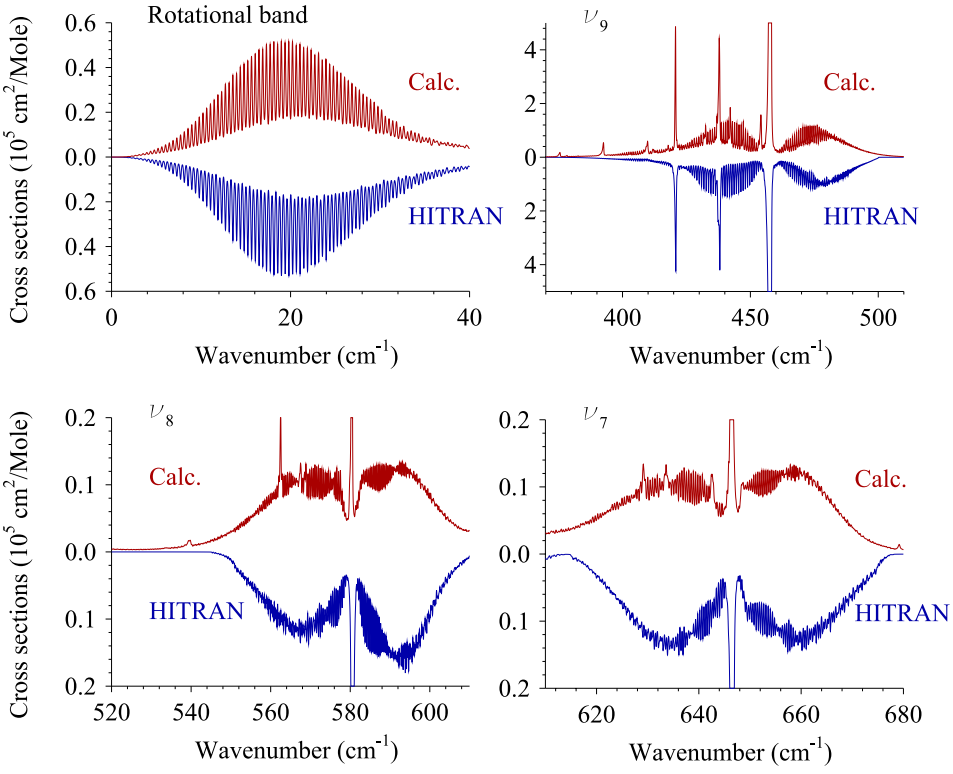

FIG. 5. Comparison of the main bands in HITRAN below 700 cm^{-1}: calculated (red curve) and HITRAN (blue curve).

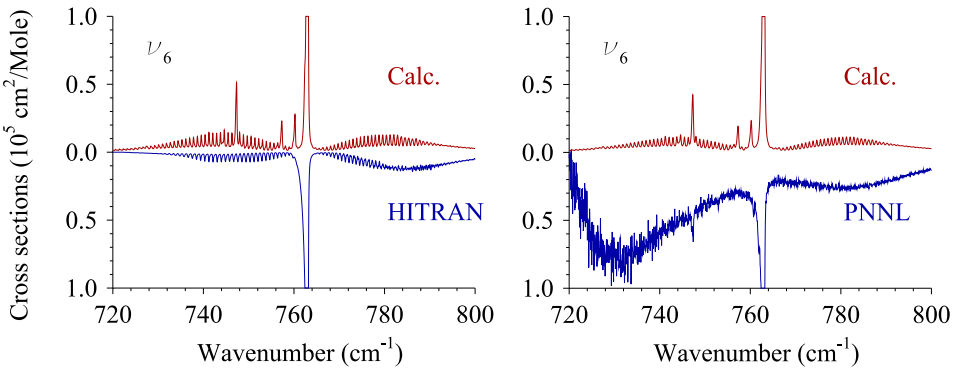

FIG. 6. Comparison of spectra for ν_6 band regions: calculated (red curve) and experimental HITRAN/PNNL (blue curve).

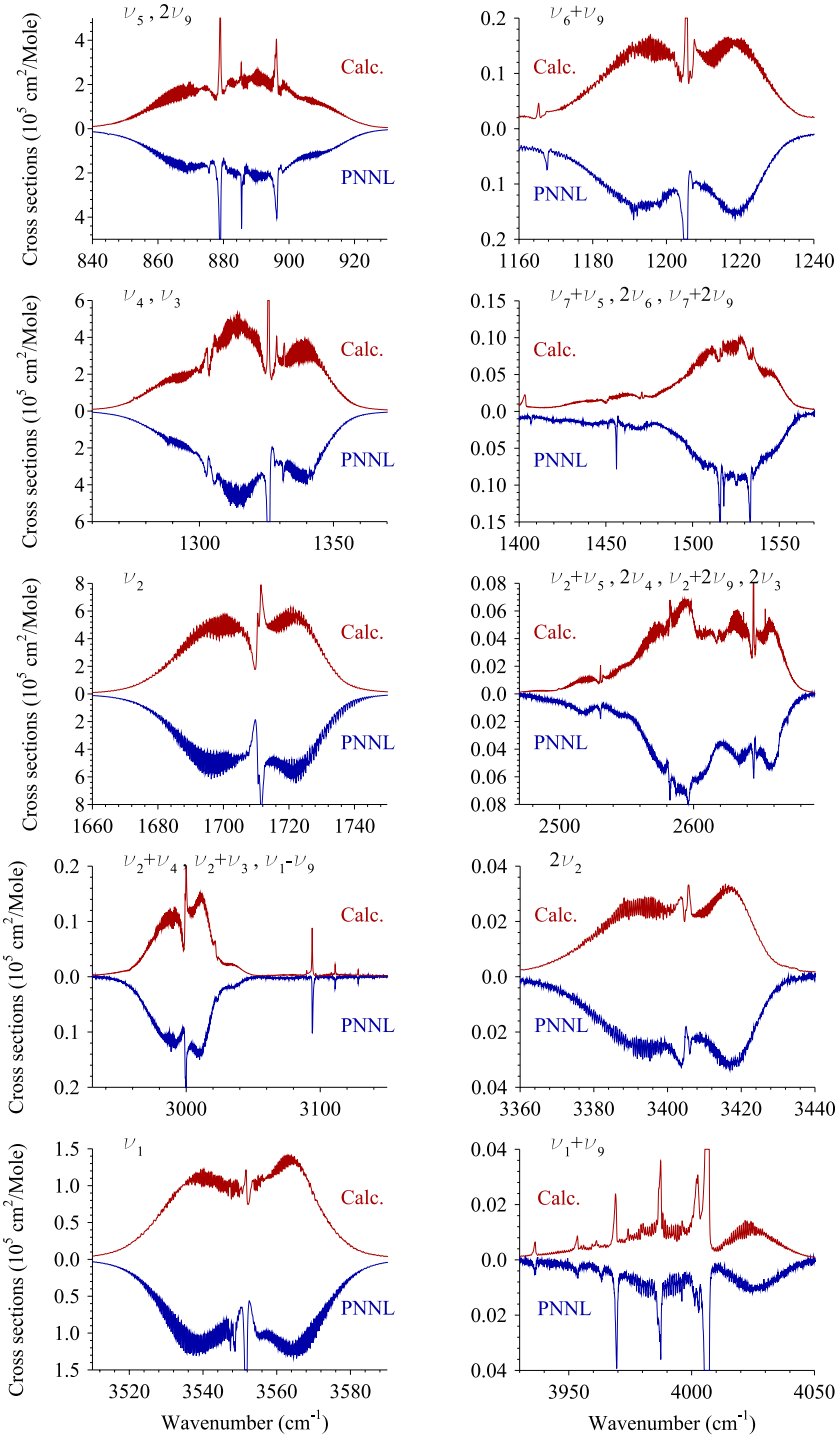

FIG. 7. Calculated (red curve) and experimental PNNL (blue curve) spectra in the region of the fundamental, first overtone, and lowest combination bands.

In this case, the DMF parameters $\vec{D}^0$, $\vec{d}_i$, and $\vec{d}_{ij}$ of Eq. (37) were varied to achieve the best agreement between theoretical and experimental integrated transition intensities for a given spectral region. This fit was again conducted using the method of regularization. We used experimental cross sections from the PNNL database[81] as input data. In the low-frequency region, which is absent from the PNNL spectrum, we used data from HITRAN.[7] In the high-frequency region 4200-7000 cm^{-1}, where the PNNL spectra are very noisy, we used the experimental intensities of Feierabend *et al.*[43] It should be noted that Feierabend *et al.* give only relative intensities, where the ν_1 band intensity was taken as unity. For this region, Table V gives absolute intensities obtained by multiplying the relative intensities of Feierabend *et al.* by the absolute intensity of the ν_1 band from PNNL. Absolute intensity values for PNNL[81] were obtained by integrating the PNNL absorption cross sections. Whenever possible, we sought not only to have the best agreement between the calculated and experimental integral intensities for a given spectral range but also good agreement between the intensities of individual transitions within each of the spectral bands. In the case of complex absorption bands, which are formed from the superposition of several intense bands, we used those intensities which gave the best fit between the experimental and calculated shape of the absorption band.

Table V shows experimental and calculated intensities for different frequency regions using the initial (calculation A) and fitted (calculation B) values of the parameters $\vec{D}^0$, $\vec{d}_i$, and $\vec{d}_{ij}$ in the DMF. This table shows that the use of the *ab initio* DMF leads to a systematic overestimation of the calculated intensities: by an average of 40% for the fundamentals bands and by 90% for the first overtones and first combination bands. Fitting gives greatly improved agreement between the calculated and experimental intensities. In this case, the average difference for the intensities of the fundamental transitions is only 0.3% and for the first overtone and combination bands, it is 40%. These differences between the computed and measured band intensities are within the experimental uncertainties. For example, in the region of the fundamental bands, intensities from HITRAN are on average 10% higher than the absorption cross sections given by PNNL. At the same time, the intensity of the $\nu_6 + \nu_9$ combination band is 30% less in HITRAN than PNNL. In addition, the PNNL spectrum which we used becomes very noisy for low intensity absorptions. Therefore, at present, it does not make sense to further improve the agreement between calculated and experimental intensities.

Figure 3 compares our calculated spectra for HNO_3 at 296 K with the data from HITRAN. Although, HITRAN aims to be comprehensive for atmospherically important molecules such as HNO_3, it actually contains only a few HNO_3 vibrational bands which means that HITRAN gives much less complete coverage than the measured cross sections from PNNL. In particular, HITRAN has no data for wavenumbers higher than 1900 cm^{-1}. Figure 4 give a similar overview comparison of our calculated spectrum with the 298 K PNNL cross sections.

Figure 5 presents more detailed comparisons for the main bands in HITRAN below 700 cm^{-1}. Generally, the agreement is very good. HITRAN is systematically missing data on hot bands even when they give rise to strong, sharp features. For example, the ν_9 band region is missing several, intense hot bands which are found in our calculation and which have been observed experimentally.[28] A similar situation arises for the ν_6 band, see Fig. 6. This band is the only one for which a direct comparison of HITRAN and PNNL data is possible. Again, our calculations predict sharp hot-band features which are absent from the HITRAN spectra. Despite becoming increasingly noisy at low frequencies, the strongest of these hot-band features can clearly be seen in the PNNL cross sections. It should be noted that the anharmonic character of the torsion ν_9 mode gives rise to a sequence of hot bands in the region 370–510 cm^{-1}, significantly shifted from the center of ν_9.

Figure 7 presents detailed comparisons of our calculated cross sections with those of PNNL measured at $T = 298$ K. Our spectra were converted to cross sections using a Voigt profile $\sigma = \gamma = 0.075$ cm^{-1} (a half width at half maximum (HWHM) of 0.153 cm^{-1}), chosen to match spectra from the PNNL database.[81] As can be seen, our calculated spectrum reproduces the PNNL cross sections very well both in the overall shape and magnitude of the band. This is also true for the finer details of the spectrum. For example, the 1800–2000 cm^{-1} region shows many features due to hot bands and combination bands which are generally well-represented in our calculated spectrum.

VII. LINE LIST

The data necessary to reproduce the spectrum of HNO_3 at temperatures up to 300 K in the 0-7000 cm^{-1} range have been stored in a variety of formats. In particular, we have created a line list in the ExoMol format.[83,84] The list contains transitions involving rotational quantum number J up to 70 for 9×10^6 vibration-rotation energy levels belonging to 1715 vibrational states and associated transitions probabilities, in form of Einstein A coefficients. The rotational angular momentum threshold of $J = 70$ provides a complete set of rotational energy levels up to 1050 cm^{-1}. To reduce the very large number of transitions between different ro-vibrational energy levels, we only retain those transitions for which the intensity is greater than 10^{-32} cm/mol at 296 K. In total, the line list contains about 2×10^9 transitions; it can be found on the ExoMol[83] website www.exomol.com. Key information on the calculation in form of the initial and refined coefficients of the potential and dipole moment functions can be found in the supplementary material to this article.[85]

VIII. CONCLUSION

We present a detailed study of the infrared spectrum of nitric acid. Calculations are performed using a hybrid variational-perturbation procedure which allows the whole spectrum to be calculated rapidly on a standard desktop computer. The procedure provides an *ab initio* if approximate method for computing spectra for larger molecules. Our initial calculations are based on *ab initio* values for the potential energy and dipole moment surfaces. For few electron triatomics, such *ab initio* procedures can give good results for both energies[86,87] and intensities.[88–90] However, this is not

possible at present for molecule as large as HNO_3. However, the efficiency of our method allowed us to tune both the potential energy surface and dipole moment function to available experimental data. Comparison with the experimental compilations available in HITRAN[7] and the PNNL database[81] generally gives excellent agreement. However, we find that HITRAN is systematically missing features due to hot bands, even when these are rather strong.

HNO_3 has a strong spectral signature in the earth's atmosphere which can be clearly seen from space. As such it is one of a number of species that are considered to be possible signatures of life (biosignature). To aid the detection of life outside the solar system and other studies on hot astronomical bodies, we are currently preparing a HNO_3 line list which should be valid over an extended temperature range. This line list will be published elsewhere.[91]

ACKNOWLEDGMENTS

This work was supported by the ERC under Advanced Investigator Project No. 267219.

[1]O. Ladobordowsky, J. Opt.-Nouv. Rev. Opt. **12**, 71 (1981).
[2]A. Goldman, F. J. Murcray, R. Blatherwick, J. J. Kosters, D. G. Murcray, C. P. Rinsland, J. M. Flaud, and C. Camy-Peyret, J. Geophys. Res.: Atmos. **97**, 2561 (1992).
[3]A. Goldman, C. P. Rinsland, A. Perrin, and J. M. Flaud, J. Quant. Spectrosc. Radiat. Transfer **60**, 851 (1998).
[4]O. V. Dorofeeva, V. S. Iorish, V. P. Novikov, and D. B. Neumann, J. Phys. Chem. Ref. Data **32**, 879 (2003).
[5]J. M. Flaud, G. Brizzi, M. Carlotti, A. Perrin, and M. Ridolfi, Atmos. Chem. Phys. **6**, 5037 (2006).
[6]S. Wang, R. Bianco, and J. T. Hynes, Comput. Theor. Chem. **965**, 340 (2011).
[7]L. S. Rothman, I. E. Gordon, Y. Babikov, A. Barbe, D. C. Benner, P. F. Bernath, M. Birk, L. Bizzocchi, V. Boudon, L. R. Brown *et al.*, J. Quant. Spectrosc. Radiat. Transfer **130**, 4 (2013).
[8]A. P. Cox and J. M. Riveros, J. Chem. Phys. **42**, 3106 (1965).
[9]J. P. Chevillard and R. Giraudet, J.Phys. **39**, 517 (1978).
[10]P. N. Ghosh, C. E. Blom, and A. Bauder, J. Mol. Spectrosc. **89**, 159 (1981).
[11]B. J. Van Der Veken, G. H. Pieters, M. A. Herman, and J. R. Durig, J. Mol. Struct. **80**, 467 (1982).
[12]A. G. Maki and J. S. Wells, J. Mol. Spectrosc. **108**, 17 (1984).
[13]C. R. Webster, R. D. May, and M. R. Gunson, Chem. Phys. Lett. **121**, 429 (1985).
[14]T. Giesen, M. Harter, R. Schieder, G. Winnewisser, and K. M. T. Yamada, Z. Naturfors. Sect. A-J. Phys. Sci. **43**, 402 (1988).
[15]R. A. Booker, R. L. Crownover, and F. C. De Lucia, J. Mol. Spectrosc. **128**, 306 (1988).
[16]R. A. Booker, R. L. Crownover, F. C. De Lucia, and P. Helminger, J. Mol. Spectrosc. **128**, 62 (1988).
[17]A. Goldman, J. B. Burkholder, C. J. Howard, R. Escribano, and A. G. Maki, J. Mol. Spectrosc. **131**, 195 (1988).
[18]R. L. Crownover, R. A. Booker, F. C. De Lucia, and P. Helminger, J. Quant. Spectrosc. Radiat. Transfer **40**, 39 (1988).
[19]A. Perrin, O. Ladobordowsky, and A. Valentin, Mol. Phys. **67**, 249 (1989).
[20]A. Maki, J. Mol. Spectrosc. **136**, 105 (1989).
[21]T. L. Tan, E. C. Looi, K. T. Lua, A. G. Maki, J. W. C. Johns, and M. Noel, J. Mol. Spectrosc. **149**, 425 (1991).
[22]T. L. Tan, E. C. Looi, K. T. Lua, A. G. Maki, J. W. C. Johns, and M. Noel, J. Mol. Spectrosc. **150**, 486 (1991).
[23]T. L. Tan, E. C. Looi, and K. T. Lua, Spectrochim. Acta, Part A **48**, 975 (1992).
[24]A. G. Maki and J. S. Wells, J. Mol. Spectrosc. **152**, 69 (1992).
[25]A. G. Maki, T. L. Tan, E. C. Looi, K. T. Lua, J. W. C. Johns, and M. Noel, J. Mol. Spectrosc. **157**, 248 (1993).
[26]A. Perrin, V. Jaouen, A. Valentin, J. M. Flaud, and C. Camy-Peyret, J. Mol. Spectrosc. **157**, 112 (1993).
[27]T. L. Tan, E. C. Looi, K. T. Lua, A. G. Maki, J. W. C. Johns, and M. Noel, J. Mol. Spectrosc. **166**, 97 (1994).
[28]A. Perrin, J. M. Flaud, C. Camy-Peyret, B. P. Winnewisser, S. Klee, A. Goldman, F. J. Murcray, R. D. Blatherwick, F. S. Bonomo, D. G. Muircray *et al.*, J. Mol. Spectrosc. **166**, 224 (1994).
[29]A. P. Cox, M. C. Ellis, C. J. Attfield, and A. C. Ferris, J. Mol. Struct. **320**, 91 (1994).
[30]L. H. Coudert and A. Perrin, J. Mol. Spectrosc. **172**, 352 (1995).
[31]T. L. Tan, W. F. Wang, E. C. Looi, and P. P. Ong, Spectrochim. Acta, Part A **52**, 1315 (1996).
[32]E. C. Looi, T. L. Lan, W. F. Wang, and P. P. Ong, J. Mol. Spectrosc. **176**, 222 (1996).
[33]T. M. Goyette, L. C. Oesterling, D. T. Petkie, R. A. Booker, P. Helminger, and F. C. De Lucia, J. Mol. Spectrosc. **175**, 395 (1996).
[34]C. D. Paulse, L. H. Coudert, T. M. Goyette, R. L. Crownover, P. Helminger, and F. C. De Lucia, J. Mol. Spectrosc. **177**, 9 (1996).
[35]W. F. Wang, P. P. Ong, H. F. Chen, and H. H. Teo, J. Mol. Spectrosc. **185**, 207 (1997).
[36]W. F. Wang, P. P. Ong, T. L. Tan, E. C. Looi, and H. H. Teo, J. Mol. Spectrosc. **183**, 407 (1997).
[37]F. Keller, A. Perrin, J. M. Flaud, J. W. C. Johns, Z. Lu, and E. C. Looi, J. Mol. Spectrosc. **191**, 306 (1998).
[38]A. Perrin, Spectrochim. Acta, Part A **54**, 375 (1998).
[39]A. Perrin, J. M. Flaud, F. Keller, A. Goldman, R. D. Blatherwick, F. J. Murcray, and C. P. Rinsland, J. Mol. Spectrosc. **194**, 113 (1999).
[40]H. Lucas and J. P. Petitet, J. Phys. Chem. A **103**, 8952 (1999).
[41]D. T. Petkie, T. M. Goyette, P. Helminger, H. M. Pickett, and F. C. De Lucia, J. Mol. Spectrosc. **208**, 121 (2001).
[42]D. T. Petkie, P. Helminger, R. A. H. Butler, S. Albert, and F. C. De Lucia, J. Mol. Spectrosc. **218**, 127 (2003).
[43]K. J. Feierabend, D. K. Havey, and V. Vaida, Spectrochim. Acta, Part A **60**, 2775 (2004).
[44]A. Perrin, J. Orphal, J.-M. Flaud, S. Klee, G. Mellau, H. Mader, D. Walbrodt, and M. Winnewisser, J. Mol. Spectrosc. **228**, 375 (2004).
[45]D. T. Petkie, P. Helminger, M. Behnke, I. R. Medvedev, and F. C. De Lucia, J. Mol. Spectrosc. **233**, 189 (2005).
[46]A. Perrin and R. Mbiake, J. Mol. Spectrosc. **237**, 27 (2006).
[47]I. M. Konen, E. X. J. Li, M. I. Lester, J. Vazquez, and J. F. Stanton, J. Chem. Phys. **125**, 074310 (2006).
[48]D. T. Petkie, M. Kipling, A. Jones, P. Helminger, I. R. Medvedev, M. Atsuko, M. Behnke, B. J. Drouin, and C. E. Miller, J. Mol. Spectrosc. **251**, 358 (2008).
[49]L. Gomez, H. Tran, A. Perrin, R. R. Gamache, A. Laraia, J. Orphal, P. Chelin, C. E. Fellows, and J. M. Hartmann, J. Quant. Spectrosc. Radiat. Transfer **110**, 675 (2009).
[50]D. T. Petkie, P. Helminger, I. R. Medvedev, and F. C. De Lucia, J. Mol. Spectrosc. **261**, 129 (2010).
[51]A. Perrin, J. Phys. Chem. A **117**, 13236 (2013).
[52]L. P. Giver, F. P. J. Valero, and D. Goorvitch, J. Opt. Soc. Am. B **1**, 715 (1984).
[53]W. F. Wang, E. C. Looi, T. L. Tan, and P. P. Ong, J. Mol. Spectrosc. **178**, 22 (1996).
[54]D. J. Donaldson, J. J. Orlando, S. Amann, G. S. Tyndall, R. J. Proos, B. R. Henry, and V. Vaida, J. Phys. Chem. A **102**, 5171 (1998).
[55]C. Chackerian, S. Sharpe, and T. Blake, J. Quant. Spectrosc. Radiat. Transfer **82**, 429 (2003).
[56]R. A. Toth, L. R. Brown, and E. A. Cohen, J. Mol. Spectrosc. **218**, 151 (2003).
[57]V. A. Benderskii and E. V. Vetoshkin, Russ. Chem. Bull. **48**, 2029 (1999).
[58]D. Lauvergnat and A. Nauts, Phys. Chem. Chem. Phys. **12**, 8405 (2010).
[59]G. Avila and T. Carrington, Jr., J. Chem. Phys. **134** (2011).
[60]G. Avila and T. Carrington, Jr., J. Chem. Phys. **137** (2012).
[61]T. J. Lee and J. E. Rice, J. Phys. Chem. **96**, 650 (1992).
[62]A. M. Grana, T. J. Lee, and M. Headgordon, J. Phys. Chem. **99**, 3493 (1995).
[63]Y. Miller, G. M. Chaban, and R. B. Gerber, Chem. Phys. **313**, 213 (2005).
[64]R. Bianco, S. Wang, and J. T. Hynes, J. Phys. Chem. A **111**, 11033 (2007).
[65]C. Gutle, J. Demaison, and H. D. Rudolph, J. Mol. Spectrosc. **254**, 99 (2009).
[66]M. Nonella, H. U. Suter, and J. R. Huber, Chem. Phys. Lett. **487**, 28 (2010).
[67]A. I. Pavlyuchko, S. N. Yurchenko, and J. Tennyson, "Hybrid variational-perturbation method for calculating ro-vibrational energy levels of polyatomic molecules," Mol. Phys. (published online).
[68]L. A. Gribov and A. I. Pavlyuchko, *Variational Methods for Solving Anharmonic Problems in the Theory of Vibrational Spectra of Molecules* (Nauka, Moscow, 1998) (in Russian).
[69]J. K. G. Watson, Mol. Phys. **15**, 479 (1968).
[70]A. I. Pavlyuchko and L. A. Gribov, J. Appl. Spectrosc. **46**, 82 (1987).
[71]S. N. Yurchenko, W. Thiel, and P. Jensen, J. Mol. Spectrosc. **245**, 126 (2007).
[72]C. G. J. Jacobi, Crelle's J. **1846**(30), 51 (1846) (in German).

[73]J. H. Wilkinson, *The Algebraic Eigenvalue Problem* (Oxford University Press, Oxford, UK, 1965).
[74]O. L. Polyansky, A. G. Császár, S. V. Shirin, N. F. Zobov, P. Barletta, J. Tennyson, D. W. Schwenke, and P. J. Knowles, Science **299**, 539 (2003).
[75]H.-J. Werner, P. J. Knowles, G. Knizia, F. R. Manby, and M. Schütz, WIREs Comput. Mol. Sci. **2**, 242 (2012).
[76]M. J. Frisch, G. W. Trucks, H. B. Schlegel, G. E. Scuseria, M. A. Robb, J. R. Cheeseman, G. Scalmani, V. Barone, B. Mennucci, G. A. Petersson *et al.*, GAUSSIAN 09, Revision D.01, Gaussian, Inc., Wallingford, CT, 2009.
[77]A. N. Tikhonov and V. Y. Arsenin, Bull. Am. Math. Soc. (N.S.) **1**, 521 (1979).
[78]L. A. Gribov and V. A. Dementiev, J. Appl. Spectrosc. **56**, 709 (1992).
[79]S. N. Yurchenko, M. Carvajal, P. Jensen, F. Herregodts, and T. R. Huet, Chem. Phys. **290**, 59 (2003).
[80]L. Lodi and J. Tennyson, J. Phys. B: At., Mol. Opt. Phys. **43**, 133001 (2010).
[81]S. W. Sharpe, T. J. Johnson, R. L. Sams, P. M. Chu, G. C. Rhoderick, and P. A. Johnson, Appl. Spectrosc. **58**, 1452 (2004).
[82]S. N. Yurchenko and J. Tennyson, Mon. Not. R. Astron. Soc. **440**, 1649 (2014).
[83]J. Tennyson and S. N. Yurchenko, Mon. Not. R. Astron. Soc. **425**, 21 (2012).
[84]J. Tennyson, C. Hill, and S. N. Yurchenko, "6th international conference on atomic and molecular data and their applications ICAMDATA-2012," AIP Conf. Proc. **1545**, 186–195 (2013).
[85]See supplementary material at http://dx.doi.org/10.1063/1.4913741 for initial and refined coefficients of the potential and dipole moment functions.
[86]M. Pavanello, L. Adamowicz, A. Alijah, N. F. Zobov, I. I. Mizus, O. L. Polyansky, J. Tennyson, T. Szidarovszky, A. G. Császár, M. Berg *et al.*, Phys. Rev. Lett. **108**, 023002 (2012).
[87]O. L. Polyansky, R. I. Ovsyannikov, A. A. Kyuberis, L. Lodi, J. Tennyson, and N. F. Zobov, J. Phys. Chem. A **117**, 9633–9643 (2013).
[88]L. Lodi, J. Tennyson, and O. L. Polyansky, J. Chem. Phys. **135**, 034113 (2011).
[89]A. Petrignani, M. Berg, A. Wolf, I. I. Mizus, O. L. Polyansky, J. Tennyson, N. F. Zobov, M. Pavanello, and L. Adamowicz, J. Chem. Phys. **141**, 241104 (2014).
[90]O. L. Polyansky, K. Bielska, M. Ghysels, L. Lodi, N. F. Zobov, J. T. Hodges, and J. Tennyson, "High accuracy CO_2 line intensities determined from theory and experiment," Phys. Rev. (submitted).
[91]A. I. Pavlyuchko, S. N. Yurchenko, and J. Tennyson, "ExoMol line lists XII: A Hot Line List for nitric acid," (unpublished).